**Intuitive Understanding of σ Delocalization in Loose and σ Localization in Tight Helical Conformations of an Oligosilane Chain**

Milena Jovanovic,[a,b] Dean Antic,[a] David Rooklin,[a] Annika Bande [a,c] and Josef Michl*[a,b]

**Abstract**. Conformational effects on σ-electron delocalization in oligosilanes are addressed by Hartree-Fock and time-dependent density functional theory (B3LYP, 6-311G**) at MP2 optimized geometries of permethylated uniformly helical linear oligosilanes (all-ω-$Si_nR_{2n+2}$) up to $n$ = 16 and for backbone dihedral angles ω = 55 - 180°. The extent of σ delocalization is judged by the partition ratio of the highest occupied molecular orbital and is reflected in the dependence of its shape and energy and of UV absorption spectra on $n$. The results agree with known spectra of all-transoid conformers (all-[±165]-$Si_nMe_{2n+2}$) and reveal a transition at ω = ~90° from the "σ-delocalized" limit

[a] Ms. M. Jovanovic
Dr. D. Antic
Dr. D. Rooklin
Dr. A. Bande
Prof. J. Michl
Department of Chemistry and Biochemistry
University of Colorado
Boulder, CO 80309-0215, USA
Josef.Michl@colorado.edu

[b] Ms. M. Jovanovic
Prof. J. Michl
Institute of Organic Chemistry and Biochemistry
Academy of Sciences of the Czech Republic
Flemingovo nám. 2
16610 Prague 6
Czech Republic

[c] Dr. A. Bande
Institute of Methods for Material Development
Helmholtz-Zentrum Berlin für Materialien und Energie GmbH
Albert-Einstein-Str. 15
D-12489
Berlin, Germany

Supporting information for this article is given via a link at the end of the document.

at $\omega = 180^\circ$ toward and close to the physically non-realizable "σ-localized" limit $\omega = 0$ with entirely different properties. The distinction is also obtained in the simple Hückel Ladder H and C models of σ delocalization. An easy intuitive way to understand the origin of the two contrasting limits is to first view the linear chain as two subchains with alternating primary and vicinal interactions (σ-hyperconjugation), one consisting of the odd and the other of the even σ(SiSi) bonds, and then allow the two subchains to interact by geminal interactions (σ conjugation).

**Introduction**

The delocalization of σ electrons is more complicated and less well understood than the delocalization of π electrons, primarily because more than one orbital participates at most atomic centers. Its effects dominate optical properties of σ-bonded structures and extend to many others, such as ionization potential, charge and energy transfer, spin density propagation, and chemical reactivity. A striking example of the effects of σ-electron delocalization is provided by the optical properties of peralkylated linear polysilanes, fully saturated chains with an all-silicon backbone.[1-4] They are sensitive to backbone conformation and as a result lead to phenomena such as thermochromism,[5-9] piezochromism,[10-11] electrochromism,[12] ionochromism,[13-14] and solvatochromism.[15] Also their single-molecule electrical conductivity appears to depend on conformation.[16] In long polysilane chains conformational segmentation into individual chromophores is important for optical absorption, emission, and charge transport properties.[17-19]

The effect of backbone conformation on the electronic excitation energies of peralkylated oligosilanes is nicely illustrated by the stark contrast between the reported effects of chain-length extension in chains kept in an all-transoid conformation [*t*] and those held in an alternating cisoid,anti conformation [*ca*] (Chart 1; in either measurement, the sense of chain helicity varies

randomly along the chain). As shown in Figure 1, an extension of the SiSiSiSi backbone from four to ten silicon atoms lowers the excitation energy of the first σσ* excitation by 9 000 $cm^{-1}$ (232 to 293 nm) in the former case,[20] whereas in the latter, it makes no difference at all, and the excitation energy remains steady at ~41000 $cm^{-1}$ (~243 nm).[21] The former result is well reproduced by TD B3LYP/TZ//MP2/TZ calculations[4,22] (TZ = 6-311G**). As we plan to report elsewhere in more detail, the latter is as well.

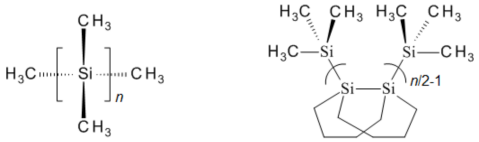


ω(SiSiSiSi): *a* = 180°; *t* = 163°; *c* = 32.9°

all-*t*-**1**[*n*]

all-[*ca*]-**1**[*n*]

$Si_n(CH_3)_{2n+2}$

even *n*

all-[*ca*]-**2**[*n*]

**Chart 1**. Structural formulas of peralkylated oligosilanes.

The contrast shown in Figure 1 provided the motivation for the present study, in which we consider the particularly simple optimized regularly helical oligosilane conformations with all backbone dihedral angles nearly identical. We use this vehicle to address the general issue of conformational dependence of σ delocalization, and particularly the widespread feeling that all-anti saturated chains σ-delocalize best, whereas gauche kinks in the chain hinder delocalization. Our

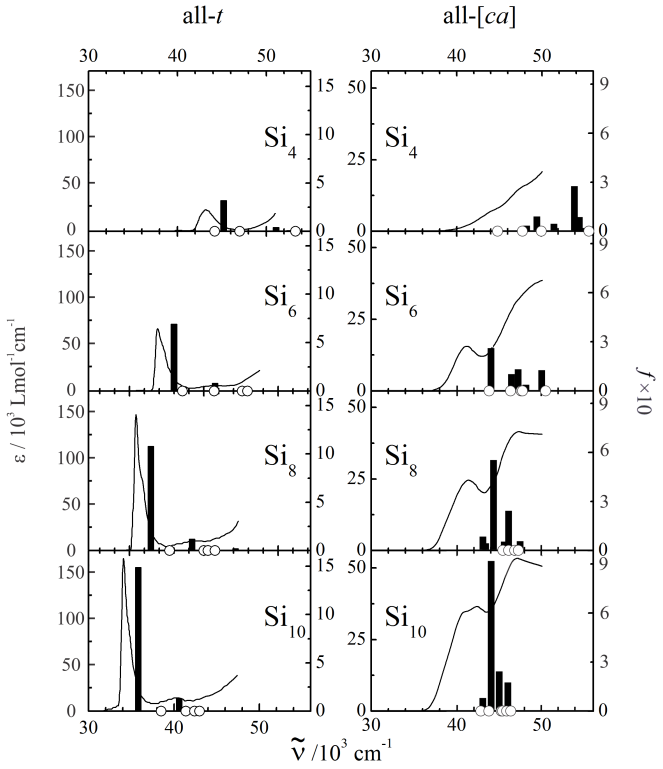


**Figure 1**. Absorption spectra and calculated ten lowest singlet-singlet transition energies and oscillator strengths (TD B3LYP/TZ, gas phase). Left: measured for all-$t_{\pm}$-**1[*n*]** (*n* = 4 - 10) in cyclopentane-isopentane (3:7 v/v) at 77 K and calculated for all-$t_{+}$-**1[*n*]**. Right: measured for all-[$c_{\pm}a$]-**2[*n*]** in tetrahydrofuran at room temperature, and calculated for all-[$c_{+}a$]-**1[*n*]**. Reprinted with permission from ref. 21. Copyright 2003 American Chemical Society.

computations rely primarily on the TD B3LYP/TZ method, which reproduces conformational effects on oligosilane electronic spectra. Our ultimate objective, simple intuitive understanding of the origin of the difference between "σ-delocalized" and "σ-localized" conformations, is achieved by the use of simplified models that successfully reproduce the properties obtained from all-electron calculations for the highest occupied molecular orbital (HOMO). In the molecular orbital (MO) approximation, the HOMO determines the ionization potential and the distribution of positive charge when the chain is doped with a hole, and the dependence of its properties on the chain length provides a reliable measure of the degree of σ delocalization. We use the Hückel Ladder H[19] (considering four hybrids on each silicon atom and one on each hydrogen or alkyl substituent) and the even simpler Ladder C[19,23-24] (considering only the two backbone-building hybrids on each silicon) models for closer examination, and find that an inspection of wave functions in both conformational limits, ω = 180 and 0°, provides an especially informative view. In reality and in DFT or Hartree-Fock (HF) calculations, steric hindrance prevents us from reaching the all-syn limit ω = 0° for $n > 4$, but in the Ladder models, it does not. Finally, we note that the Ladder C model is already known[25] to account for the strong effect of conformation on the red shift of the σσ* transition that is induced by doubling the number of SiSi bonds in an oligosilane (the attribution of σ and π character to MOs of a saturated chain is discussed below). A similarly simple procedure is currently not available for σπ* transitions.

The Methods and Results parts of the paper are organized accordingly. (i) We start with a brief overview of σ-electron delocalization and its relation to σ conjugation. (ii) We provide a description of computational procedures used and describe a simple modification of the method we proposed earlier[25] for assigning fractional σ and π character to backbone orbitals and a degree of

σσ* and σπ* nature to the excited states of non-planar oligosilane conformers. The modified definition is better adapted to chains capable of attaining planarity than the original version was. (iii) We use the mostly hypothetical regular helical conformations as the simplest archetypical model appropriate for a saturated chain and characterize their spectral and HOMO energies as a function of chain length and dihedral angle by TD DFT and HF calculations. (iv) We find that qualitatively identical results for HOMO energies are obtained with the simple Hückel Ladder H and even Ladder C models, suggesting that the striking difference between loose and tight helical conformers is a deep-seated property of σ delocalization. (v) We provide a simple intuitive explanation of the origin of this difference in terms of the Ladder C model.

The present study is confined to the examination of regularly helical oligosilane conformations, all-[ω]-**1[*n*]**. We plan to publish separately the results of two related investigations: (i) the properties of the alternating cisoid,anti conformations all-[*ca*]-**1[*n*]** and **2[*n*]** (Chart 1 and Figure 1); (ii) a more rigorous analysis of the band structure for both types of conformation in the limit of infinite chains, where we examine the range of validity of the present conclusions regarding the effect of backbone dihedral angles on σ delocalization as we vary the backbone chemical element, bond length, and valence angle.

**Methods and Results**

We have performed DFT calculations for the evenly helical conformations of permethylated oligosilanes (all-ω-$Si_nMe_{2n+2}$, **1[*n*]** in Chart 1) from $n$ =2 to $n$ = 16, starting with the planar zig-zag all-anti chain limit (ω = 180°) through loose helices (ω = 180 - 100°), tight helices (ω < 100°), and as close to ω = 0° as conveniently possible before steric hindrance becomes excessive. We use

permethylated oligosilanes rather than the unsubstituted parent oligosilanes (all-ω-$Si_nH_{2n+2}$), likely to reveal the same principles, because we want to compare our results with already published experiments on helices in which the degree of helicity is regular (but its sense random). Unlike the perfectly stable peralkylated oligosilanes for which much information is available, the parent oligosilanes are unstable, pyrophoric, and rarely studied.[26]

**(i) σ Delocalization**

As discussed in more detail elsewhere,[25] we use this term in saturated molecules such as alkanes and oligosilanes to describe the deviation of electronic structure from that implied by a single Lewis formula. Such a formula represents a collection of perfectly localized primary σ bonds between neighboring Si atoms, formed by atomic hybrid orbitals pointing at each other. These orbitals are conveniently thought of as Löwdin orthogonalized Weinhold's natural hybrid orbitals (NHOs)[27] and are close to $sp^3$, as discussed elsewhere.[28] The two-electron two-center bonds can be described by valence-bond (VB) or molecular orbital (MO) wave functions. In discussions of interactions between these perfectly localized bonds that lead to σ delocalization it is common to use the less accurate but simpler MO picture and we shall do so in the following.

Interactions between perfectly localized bonds can produce partial bond delocalization, and its nature is dictated by the topology of the overlaps of the participating NHOs in a manner that is more complicated than in π-electron systems, where linear, cyclic, spherical, tubular, and cross conjugation are the five main representatives. Depending on the topology provided, electron delocalization affects various molecular properties to different degrees. It is common to call a system σ-delocalized if its extension causes a red shift of the HOMO-LUMO transition and a large

decrease in the ionization potential, and to call it "σ-localized" if it does not do so to a significant extent.

A quantitative measure of delocalization of an electron or a hole in a normalized orbital *i* suitable for our purposes is the partition ratio $p_i$, defined as

$$p_i = 1/(m\Sigma_{\mu=1}^{\mu=m} c^4_{\mu i}) \quad (1)$$

where $m$ is the number of sites and $c_{\mu i}$ is the amplitude of orbital $i$ on site μ.[29] In a perfectly delocalized orbital $i$, in which all $c^2_{\mu i}$ values are equal, $p_i = 1$. In a perfectly localized orbital $i$, in which $c^2_{\mu i}$ equals unity at one of the sites μ and zero at all the others, $p_i = 1/m$.

In a traditional usage of the terms[25] (which is not accepted generally[30-31]), the system is σ-conjugated if the deviation from strict bond localization is due to geminal interactions (those between hybrid orbitals located on the same atom), σ-hyperconjugated if it is due to vicinal interactions (those between hybrid orbitals located on neighboring atoms with neither pointing at the other atom, often referred to as "through-bond coupled"), and σ-homoconjugated if it is due to interactions between hybrid orbitals located on non-neighboring atoms (sometimes called "through-space coupled"). Interactions between hybrids on neighboring atoms chosen such that one points at the other atom, and the other does not, are considered less important and do not seem to have a name. In real systems the various types of conjugation act simultaneously and coherently to delocalize the σ electrons, but one of them often predominates. We shall see below that the interplay of geminal interactions (σ conjugation) and vicinal interactions (σ hyperconjugation) is especially important. The historical term σ conjugation for the geminal interaction and the corresponding term

σ hyperconjugation for vicinal interaction may be somewhat unclear for a beginner and it would probably be better to use the more descriptive terms geminal and vicinal conjugation. In the following we try to list both to minimize confusion.

Attempts to obtain simple intuitive understanding of σ delocalization with a minimum of computation are usually based on the one-electron (Hückel) level of theory. Ordinary Extended Hückel Theory (EHT), in which each atomic orbital is allowed to interact with all others, contains too many interactions to serve the purpose conveniently. Simplified Hückel models for alkanes (later applied to oligosilanes), which consider only σ conjugation, were devised by Sandorfy[32] and were subsequently generalized to the Pariser-Parr-Pople (PPP) level by adding electron repulsion.[33] In Sandorfy's model H, all hydrogen and carbon (or silicon) orbitals are considered, but it has been rarely if ever used to gain simple intuitive insight, because it is still very complex. Sandorfy model C for alkanes (or oligosilanes), which considers only two orbitals on each carbon (or silicon) within a chain, is more suitable. However, both Sandorfy models are oversimplified for our purposes, since they give the same result for all conformations of a molecule. For treatment of conformational effects, inclusion of vicinal effects (σ hyperconjugation) is essential.

A useful model simple enough for qualitative understanding of linear σ-delocalized chains and often adequate for interpretations is the Ladder C,[19,23-24] which resembles Sandorfy model C by considering only two backbone hybrid orbitals on each carbon (or silicon), but which includes both geminal interactions (σ conjugation) and vicinal interactions (σ hyperconjugation). Unlike the resonance ("hopping") integrals $\beta_p$ and $\beta_g$, which describe the primary and the geminal interactions among the NHOs, respectively, the resonance integrals $\beta_v$ that describe the vicinal interactions introduced by the Ladder C model depend on backbone dihedral angles in magnitude and even in

sign. This very simple model is capable of describing the intrinsically cyclic nature of σ delocalization in a linear saturated chain by introducing an interplay of geminal and vicinal interactions as a function of conformation. The reader is referred elsewhere[25] for additional detail. Unlike the rather complicated Ladder H model, the Ladder C model pretends that π orbitals and σπ* excitations do not exist and is useful for intuitive understanding of the behavior of σ orbital and σσ* excitation energies.

**(ii) Methods of Calculation**

Chart 1 displays the structural formulas of the oligosilanes of interest. Structures all-*t*-**1[4]** to all-*t*-**1[16]** represent the regular helical geometries of the all-*t*-$Si_nMe_{2n+2}$ permethylated oligosilanes with a backbone dihedral angle ω ≈ 163° along the entire chain length and are dealt with presently. The structures [*c*]-**2[4],** all-[*ca*]-**2[6],** all-[*ca*]-**2[8]**, and all-[*ca*]-**2[10]** have alternating SiSiSiSi backbone dihedral angles ω and ω', where the cisoid angle is constrained to ω = 32.9° and the anti angle to ω' = 180°, and will be dealt with elsewhere. Both sets of structures are defined as regular helices with chain lengths *n* = 4 - 16 and 4 -10, respectively (the samples for which experimental data are available undoubtedly have a random distribution of helical sense along the chain).

The ground state geometries of all-*t*-**1[2*m*]** (*m* = 2 - 8) and all-*t*-**1[2*m*+1]** (*m* = 2 - 4) were optimized at the MP2/6-311G** (TZ) level of theory subject to the angular constraints stated, using the RI approximation in the Turbomole program package.[34] In our past experience, MP2 optimized and DFT optimized geometries are very similar, but when it comes to dihedral angles, the former agree a little better with experiment, presumably because they include dispersion interactions. We

use MP2 geometries but expect that the conclusions would not change if we used DFT geometries instead.

Geometries of other nearly regularly helical ground-state conformations of linear permethylated oligosilanes of chain lengths extending from $n = 4$ to $n = 16$ were optimized at the same level of theory. This caused the dihedral angles within the same molecule to deviate by 1 - 2° from each other, and we checked that this made no difference in the results. Optimized conformers exhibiting nearly regular helical patterns along the silicon backbone[35] were all-gauche (*g*; ω ≈ 55°), all-ortho (*o*; ω ≈ 90°), all-eclipsed (*e*; ω = 120°), all-deviant (*d*; ω = 150°), all-transoid (*t*; ω ≈ 163°), and all-anti (*a*; ω = 180°). For $n = 16$, we also optimized the all-cisoid conformation (*c*; ω ≈ 37°). From earlier work,[12-13,15,20] the *g*, *o*, and *t* conformations at internal SiSi bonds are known to represent local minima on the potential energy surfaces of short permethylated oligosilanes, and chains substituted with longer alkyls occasionally show additional minima at *c* and *d* conformations. The optimization of the *e*, *d*, and *a* conformations, which do not correspond to minima in the potential energy surface of permethylated oligosilanes, was constrained in that the dihedral angles were set equal to the values specified above. Odd-numbered chain lengths from $n = 5$ to $n = 15$ were constructed by extending the optimized even-numbered chains by one trimethylsilyl group at the proper dihedral angle ω, and the resulting geometries were symmetrized prior to performing single-point energy calculations at the HF/6-311G** (HF/TZ) and B3LYP/6-311G** (DFT/TZ) levels, using Gaussian 03W.[36]

Excitation energies and oscillator strengths were calculated by the TD DFT (RPA) procedure[37] using the B3LYP/TZ (TD DFT/TZ) method in the Gaussian 03W or Gaussian 09[38] program suite. TD DFT (TDA) results were also obtained for all six conformations of $Si_8Me_{18}$ and

were virtually identical, with excitation energies differing by less than 0.05 eV, oscillator strengths by less than 20%, and the amplitudes of various electron promotions by less than 2%. NHOs of all molecules were calculated using the Gaussian NBO versions 3.1 and 5.0[39-40] and the amplitudes of MOs in the NHO basis were used to compute percent σ and π character of an MO according to published[25] formulas, modified slightly as described below. The percent σσ* and σπ* character of an excitation was determined as a weighted average of σσ* and σπ* contributions provided by each MO pair contributing to the excitation, respectively.

A modification of the original procedure[25] for determining the percent σ and π character of a molecular orbital that has been introduced presently changes only the contributions provided by terminal $SiMe_3$ groups. It makes the definition more compatible with standard usage for chains whose backbone can achieve planarity. Now, not only all of the *A* symmetry, but also half of the *E* symmetry contribution of terminal $SiMe_3$ counts toward σ character, while the other half of the *E* symmetry contribution counts toward π character. To achieve this, equations (12) in ref. 25 have been modified from the original

$$s_{\kappa,\lambda} = s_{\kappa,\lambda'\lambda''\lambda'''} = c_{\kappa A}^2/(c_{\kappa A}^2 + c_{\kappa E1}^2 + c_{\kappa E2}^2) \quad (2)$$

$$p_{\kappa,\lambda} = p_{\kappa,\lambda'\lambda''\lambda'''} = (c_{\kappa E1}^2 + c_{\kappa E2}^2)/(c_{\kappa A}^2 + c_{\kappa E1}^2 + c_{\kappa E2}^2) \quad (3)$$

to the newly adopted

$$s_{\kappa,\lambda} = s_{\kappa,\lambda'\lambda''\lambda'''} = (c_{\kappa A}^2 + c_{\kappa E1}^2)/(c_{\kappa A}^2 + c_{\kappa E1}^2 + c_{\kappa E2}^2) \quad (4)$$

$$p_{\kappa,\lambda} = p_{\kappa,\lambda'\lambda''\lambda'''} = c_{\kappa E2}^2/(c_{\kappa A}^2 + c_{\kappa E1}^2 + c_{\kappa E2}^2) \quad (5)$$

Excitation energy surfaces of regular oligosilane helices $Si_nMe_{2n+2}$ were plotted as a function of chain length *n* and backbone SiSiSiSi dihedral angle ω and their color indicates either the oscillator strength per Si atom, *f/n*, or the percent of σσ* character. They were obtained by spline interpolation between the grid points for which calculations were performed, using a 6° mesh size. The color mapping of the surface was handled automatically within Matlab®[41] by linear interpolation along the two directions of the surface plane. The surrounding grid points were assigned a value of the RGB code.

The parameters used in the Hückel calculations were (in eV)[19]: Ladder C, $\alpha_{Si}$ = -6.1, $\beta_p$ = -3.5, $\beta_g$ = -1.1, $\beta_v$ = 0.11 - 0.70×cosω; Ladder H, $\alpha_{Si}$ = -6.5, $\alpha_C$ = -9.6, $\beta_p$ = -3.2, $\beta_{SiR}$ = -3.8, $\beta_g$ = -1.8, $\beta_v$ = -0.28 - 0.99×cosω. In the calculation of the partition ratio $p_i$ of a molecular orbital *i* in the Ladder C model the *m* sites are identical with the *m* members of the NHO basis set.

**(iii) σ-Delocalized and σ-Localized Conformers**

The left-hand side of Figure 1 compares the low-temperature UV absorption spectra of the linear permethylated oligosilanes $Si_nMe_{2n+2}$ (*n* = 4, 6, 8, and 10),[24,42-48] believed to be due to the all-*t* conformers with a randomly distributed helicity sense,[4] with the transition energies and oscillator strengths calculated (TD DFT/TZ) for the all-*t* conformers all-*t*-**1[4]** to all-*t*-**1[10]**. The only observed intense absorption maximum gradually shifts from 43 100 $cm^{-1}$ in $Si_4Me_{10}$ to 34 100 $cm^{-1}$ in $Si_{10}Me_{22}$, and gains a factor of nearly 10 in intensity in the process. The long-axis polarized excitations to the first and only calculated strongly allowed excited state of *B* symmetry are in good agreement with the positions of the intense bands apparent in the observed absorption spectra. All calculated energies are slightly too high (perhaps due to solvent effects). A series of much weaker

additional transitions is calculated to be present. Only one of them has significant intensity and is actually observed, while the rest would not be expected to be easily detectable. In peralkylated *n*-tetrasilanes, whose spectra have been studied in considerable detail at a series of conformations, these additional transitions have been uncovered and are in impressive agreement with the results of TD DFT/TZ, CAS-PT2, and SAC-CI calculations.[4,22,25] A less detailed study is available for a few conformers of peralkylated hexasilanes.[49]

The right-hand side of Figure 1 serves only for highlighting the contrast between a σ-delocalized and a σ-localized behavior and will be dealt with in more detail elsewhere. It displays the reported UV absorption spectra of the alternating polycyclic oligosilanes all-[*c*]-**2[4]** to all-[*ca*]-**2[10]**),[21] again with a randomly distributed helicity sense, in which the purpose of the additional alkane chains is to impose on the silicon backbone the geometry of the desired conformation. Along with these spectra, Figure 1 shows the results of TD DFT/TZ calculations for the permethylated linear analogues of the these polycyclic oligomers ([*c*]-**1[4]** to all-[*ca*]-**1[10]** in Chart 1, with uniform helical sense). In this series of oligosilanes, there is no red shift in the observed primary absorption maximum with increasing chain length and it remains near 41 000 $cm^{-1}$ ([*c*]-**2[4]** is not a true member of the series since it has only one backbone dihedral angle). The results of the calculations reproduce the observed absence of a trend well, but all calculated excitation energies are too high.

***Regular Helical Oligosilanes.*** Figure 2 shows the TD DFT/TZ surfaces of excitation energy from the 1*A* ground state to the four lowest-lying singlet excited states of permethylated $C_2$ symmetry oligosilanes as a function of the number *n* of Si atoms in the chain and of the SiSiSiSi backbone dihedral angle ω. Plotting against 1/*n* instead of *n* permits a nearly linear extrapolation of the rapidly dropping energy of the 1*B* transition to $n = \infty$. Higher energy calculated transitions

are not considered reliable because of the intervention of Rydberg states and are not shown.

In the following, we describe the calculated excitations approximately, using the TD DFT excitation amplitudes, since this is adequate for our purposes. The starting MO for all electron promotions involved in the transitions shown is of σ character, but the terminating orbital can be mostly σ*, mostly π*, or strongly mixed. The color of each surface in Figure 2 reflects the calculated percent σσ* character of the transition. The σσ*/σπ* character of the excited state is strongly mixed at most points in the (ω,*n*) space.

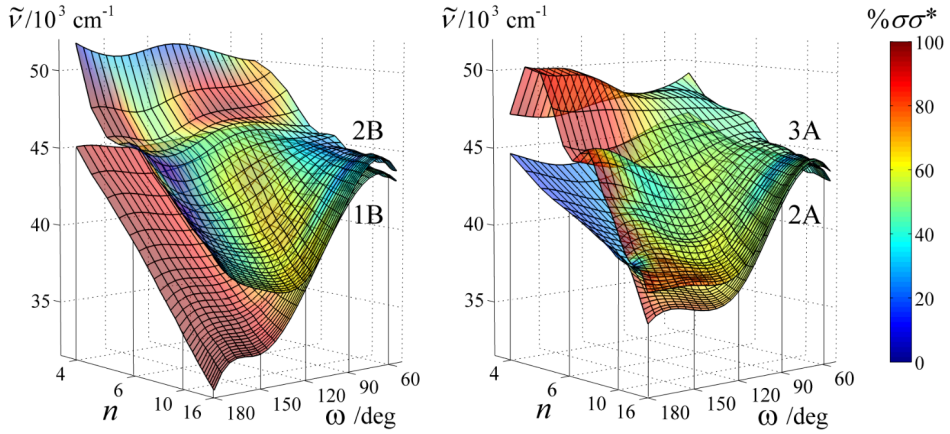


**Figure 2**. TD DFT B3LYP/TZ transition energy surfaces of the four lowest lying singlet excitations in all-[ω]-**1[*n*]** (*n* = 4 - 16). Left, states of *B* symmetry, right, states of *A* symmetry. The color scale indicates the percent σσ* character of the excited state.

Figure S1 (Supporting Information) shows the same plot in which color is used to show the computed oscillator strength. Only some transitions into states of *B* symmetry have significant intensity and those into *A* states are all very weak. The intensity is associated with the weight in the excitation of that σσ* promotion in which σ and σ* resemble the HOMO and the lowest energy virtual σ* MO at ω = 180° (see below). At ω values close to 180°, this promotion contributes

almost exclusively to the transition to the 1*B* state, which completely dominates the spectrum. Transition into the 2*B* state is of the σπ* type and is forbidden at ω = 180°. The only higher transition with noticeable intensity is a weak one into the 3*B* state, faintly seen in the absorption spectrum in Figure 1.

When ω is decreased below ω = 180°, σ*/π* mixing becomes allowed and provides increased intensity to the transition to 2*B* until ω reaches about 120°, at which point the excitation is well described as HOMO to LUMO+2. At smaller dihedral angles the intensity drops again to negligible values. In general, however, only relatively small changes occur upon going from 180° to 120° and in particular, the 1*B* state keeps its HOMO to σ* character and high intensity almost intact. The slope of $E(1B)$ against $1/n$ is gradually reduced; whereas the value of $[dE(1B)/d(1/n)]_{n=\infty}$ at 180° is $72.3\times10^3$ cm$^{-1}$, at 163° it is $62.2\times10^3$ cm$^{-1}$, at 120° it is $41.7\times10^3$ cm$^{-1}$, and at 90° it is only $16.1\times10^3$ cm$^{-1}$.

Below 120°, the picture changes entirely (Figures 2 and S1). The 1*B* state loses its σσ* character and becomes predominantly σπ*, while the σσ* character moves to the 2*B* state. The energy of all four computed transitions increases to values characteristic of the shortest chains, and it becomes essentially independent of chain length. At ω values below 90°, the energy of the 1*B* transition drops only up to $n = 6$ and then remains nearly constant in longer chains. None of the four lowest transitions have significant intensity. This has a dramatic effect on the appearance of the calculated absorption spectra, as is illustrated for $Si_{13}Me_{28}$ in Figure 3 (the peak half-width at half maximum, 700 cm$^{-1}$, was chosen to fit roughly the shape of low-temperature spectrum of all-*t*-**1[10]**[22]). Down to 150°, the transition to the 1*B* state is the strongest, but at 120°, it already only appears weakly and 2*B* with 3*B* carry far more oscillator strength. The trend continues, and the

calculated absorption spectra of all-*o* and all-*g* conformer do not show any intense absorption at low energies. The increase in the energy of the 1*B* transition, the gradual shift of oscillator strength to higher energy transitions, and the reduced separation between transitions as ω decreases are striking.

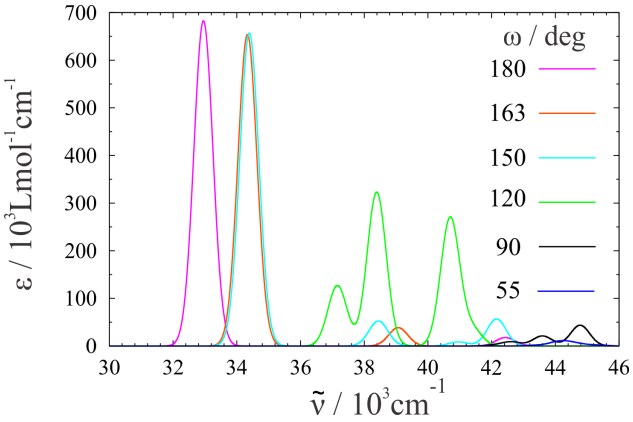


**Figure 3**. TD DFT B3LYP/TZ absorption spectra of all-*a* (pink), all-*t* (orange), all-*d* (light blue), all-*e* (green) all-*o* (black), and all-*g* (dark blue) conformers of $Si_{13}Me_{28}$. The all-*t* specrum was shifted by 100 $cm^{-1}$ to lower energies in order to avoid excessive overlap with the all-*d* spectrum.

Figures 2, S1, and 3 demonstrate that regular helical permethylated oligosilanes occur as two entirely different limiting chromophores, one with a loose helix (ω close to 180°) and one with a tight helix (ω close to 0°). As the two are interconverted, their properties correlate smoothly through avoided crossings at ω = 90 - 120°.

The difference between the two limits is in the very different degree of delocalization of the HOMO, which is always predominantly of σ character. Like all other σ(SiSi) bonding MOs, it has no nodes between Si neighbors at any ω. However, it has a node at each of them, since after all, it is the least stable of all σ(SiSi) orbitals. The contrast between the two limits is seen in Figure 4, which shows the standard representation of the HOMO of $Si_{12}Me_{26}$, and much more clearly in the

symbolic representation of the HOMO of $Si_{16}Me_{34}$ on the top of Figure 5. The all-anti HOMO is evenly distributed over the whole oligosilane chain and in that regard is reminiscent of the π HOMO of a long polyene. Near the all-syn limit the HOMO consists of a series of islands of large amplitude separated by regions of almost vanishing amplitude, and is reminiscent of those polyene MOs whose energies lie at the center of the bonding π-orbital band. Near the all-syn limit, the energies of electronic excitations in long chains therefore still only reflect those within an individual isolated island. As the chain is built by a gradual increase of *n*, the islands in the HOMO of a tight oligosilane are formed one after another. The delocalization within the first island is reflected in the response of the properties of the shortest oligosilanes to increasing *n*, but the addition of further islands makes little difference (Figure 2). The exact size of the islands into which the HOMO is divided depends on *n* and the details of the calculation, and the reason for this sensitivity will become clear below.

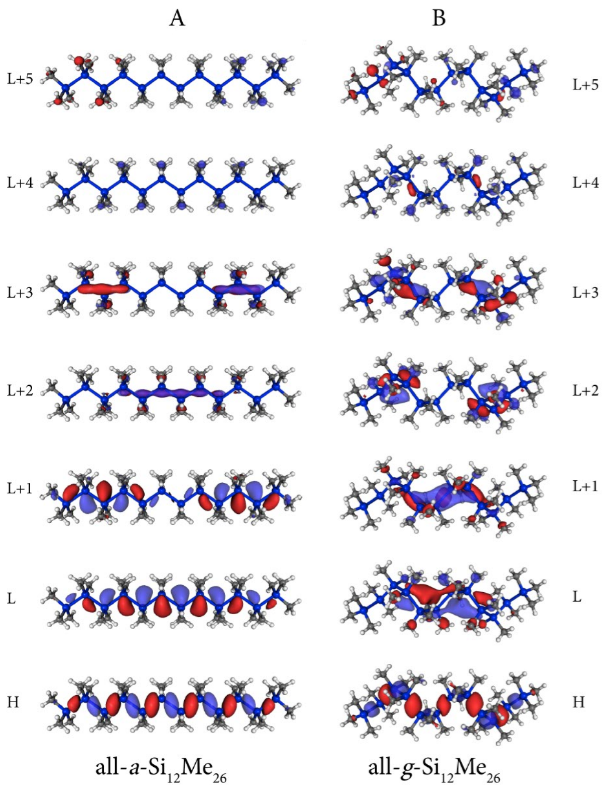


**Figure 4**. TD DFT B3LYP/TZ frontier orbitals in all-[*a*]-**1[12]** (A) and all-[*g*]-**1[12]** (B).

***Loose-Helix Oligosilanes***. With the present definition of percent σ and π character, at planar ω = 180° geometries symmetry requires each state to be either 100% σσ* or 100% σπ*. The form of the MOs involved in low-energy transitions is illustrated in Figure 4A on the example of all-*anti*-$Si_{12}Me_{26}$. The σ HOMO is the least bonding combination of σ(SiSi) bond orbitals, with geminally (σ-conjugatively) and vicinally (σ-hyperconjugatively) destabilizing nodes at every Si atom, whereas σ* is the most bonding combination of σ*(SiSi) antibond orbitals, with geminally and vicinally stabilizing interactions at every Si atom. The σ* LUMO+1 orbital contains a node at the central Si atom. The two π*(SiC) orbitals, LUMO+2 and LUMO+3, are formed by π interactions of out-of-phase combined SiC antibonds at each Si atom. The more stable LUMO+2 contains no nodes other than the one in the plane of the Si atoms, whereas the less stable LUMO+3 contains an additional node through the central SiSi bond. As usual, the amplitude of these orbitals is concentrated away

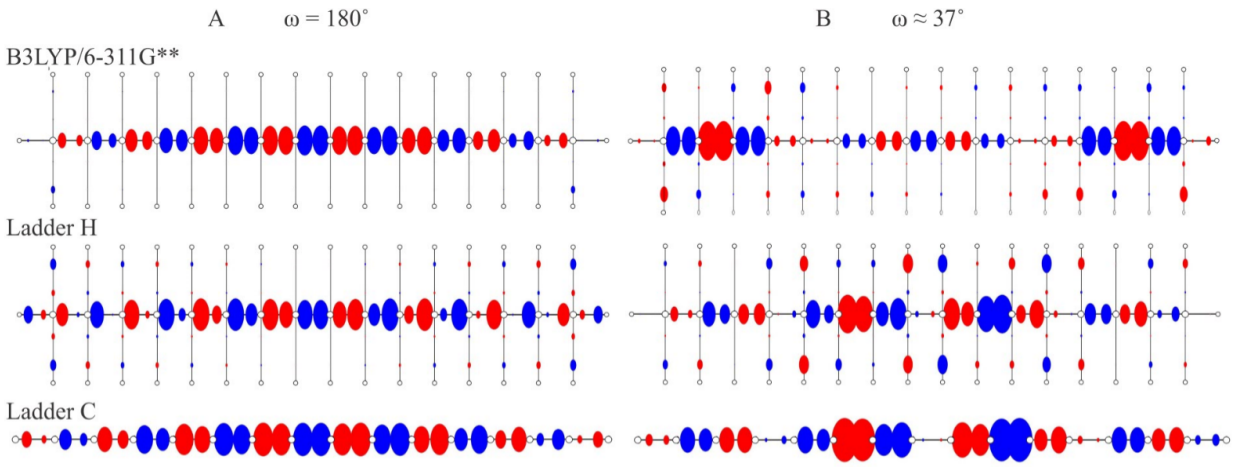


**Figure 5.** Symbolic representation of the HOMO of all-[ω]-$Si_{16}Me_{34}$ in its all-anti (A) and all-cisoid (B) conformations at three levels of approximation. Larger (smaller) empty circles stand for Si atoms (lateral substituents). Amplitudes (signs) of NHOs are shown by size (color) of ovals located next to the Si atoms and below or above the lateral substituent atoms.

from nodes. Inspection of the orbital shapes makes it very obvious why only the HOMO to LUMO excitation carries large oscillator strength.

The electronic spectra of the loose helix conformers are characterized by two low-energy electron promotions from the σ(SiSi) type HOMO, each into one of the two virtual orbitals that compete for the status of the lowest unoccupied molecular orbital (LUMO). One of them is of the σ*(SiSi) type and the strongly allowed excitation into it produces the 1*B* σσ* state. The other is of the π*(SiC) type and the very weakly allowed excitation into it produces the 2*A* σπ* state.

The oscillator strength *f* of the transition into the 1*B* state is proportional to *n*. The calculations reproduce this trend well but the absolute values of *f* are too large and the excitation energies are a little too high. They drop almost linearly with 1/*n*, with a slope of $[dE(1B)/d(1/n)]_{n=\infty} = 72.3\times10^3$ cm$^{-1}$, and extrapolate to a limit of 27 500 cm$^{-1}$ at infinite chain length and ω = 180°.

The 2*A* excited state carries negligible oscillator strength. Its energy drops only slightly less linearly with increasing *n*, but with only about half the slope, $[dE(2A)/d(1/n)]_{n=\infty} = 42.4\times10^3$ cm$^{-1}$. The 2*A* state lies below 1*B* in the shortest oligosilanes, but in all permethylated oligosilanes with more than five or six Si atoms, it lies above 1*B*. As noted above, experimental evidence for the presence of the 2*A* state is available in a trisilane, *n*-tetrasilanes and *n*-hexasilanes.

Other transitions of negligible intensity follow at higher energies. The energy of the 2*B* and 3*A* states drops rapidly with increasing *n*, and the 2*A* and 3*A* states touch near *n* = 12. At smaller values of *n*, the 2*A* state is σπ* (excitation from HOMO to π*) and the 3*A* state is σσ* (excitation from HOMO−1 to σ*). At larger values of *n*, the 2*A* state is σσ* (HOMO−1 to σ*) and the 3*A* state is well approximated as σπ* (HOMO to π*). Finally, the 2*B* state, always well separated in energy from the 1*B* state, is of σπ* nature. Its energy also drops rapidly with increasing *n* and it is possible

that in very long chains it lies below the 3*A* state.

***Tight-Helix Oligosilanes***. Steric hindrance prevents the construction of the other natural limit for the oligosilane chromophore, with a dihedral angle ω = 0°. This limit is therefore purely hypothetical and we cannot use TD DFT theory to calculate its properties, although we still can examine them in simple models such as Ladder C and Ladder H.

Using all-*gauche*-$Si_{12}Me_{26}$ as an example, Figure 4B shows the form of the molecular orbitals involved in low-energy transitions and demonstrates how dramatically they differ from the analogous orbitals in the all-*anti*-$Si_{12}Me_{26}$ conformer (Figure 4A). The contrast is even more easily seen in the symbolic representation of the MOs of $Si_{16}Me_{34}$ in Figure 5. The segmentation of the orbitals in the all-gauche case is very different from the even delocalization in the all-anti case and makes it understandable why the energy of the HOMO changes so little with chain length in the former while it increases rapidly with increasing chain length in the latter.

At ω = 55°, the σσ* character has mostly disappeared even from the 2*B* state and moved to states that are still higher in energy. It would thus appear that in the unreachable limit of ω = 0°, the σσ* excitation energy would be very high. The four lowest energy excited states are primarily σπ*. Transition oscillator strength follows the nature of the excited state, and as σ to σ* excitation character disappears from the 1*B* excitation, so does the intensity. At dihedral angles smaller than 90°, all four lowest transitions are predicted to carry nearly no oscillator strength at all.

These changes in the nature and intensity of electronic excitation are accompanied by similarly dramatic changes in transition energy. The $[dE(1B)/d(1/n)]_{n=\infty}$ slope is $13.8\times10^3$ $cm^{-1}$ at 55°. The slope for the 2*B* state ($31.2\times10^3$ $cm^{-1}$) is about twice the slope for the 2*A* state ($16.6\times10^3$ $cm^{-1}$).

**(iv) Simple Hückel Models for Loose and Tight Helices**

It is reasonable to expect the huge difference between the properties of loose and tight helical conformations of oligosilanes to be a fundamental feature, present even in the simplest models of σ delocalization. We next examine models that operate at the Hückel level: the Ladder H[19] that considers all four valence orbitals on the silicon atom as well as orbitals on substituents that are attached to the silicon backbone, and the even simpler Ladder C[19,23-24] that considers only the two valence orbitals on each silicon atom that are used to form the oligosilane backbone.

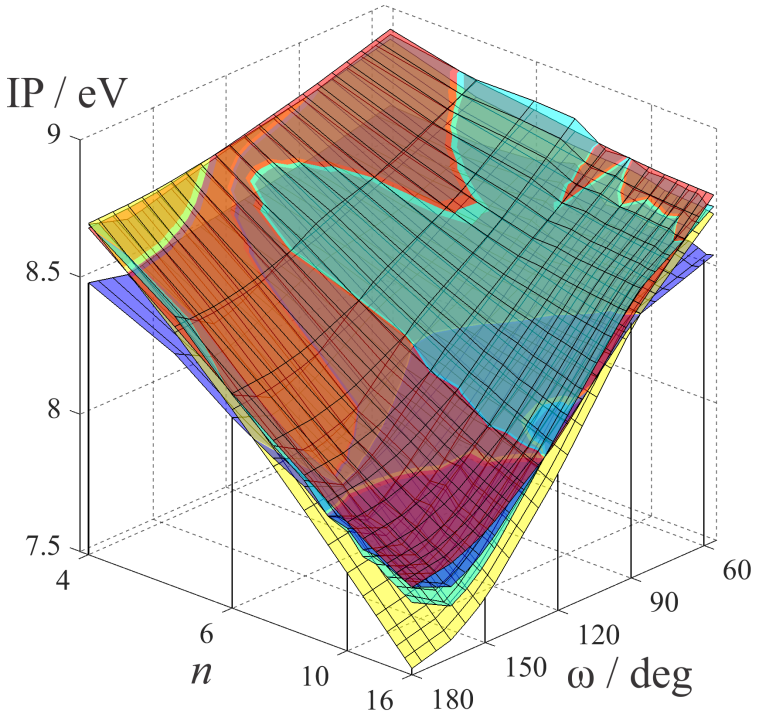


**Figure 6.** The ionization potential of all-[ω]-**1[*n*]** (*n* = 4 - 16) calculated in the Koopmans approximation with: Ladder C (red), Ladder H (yellow), HF/TZ (green), and DFT/TZ (blue, shifted up by 2.3 eV).

Figure 6 compares the HF and KS HOMO energies with those obtained with the Ladder H and C results using standard parameters[19] and demonstrates that all four methods predict qualitatively and even semiquantitatively the same dependence of the HOMO energy on $n$ and ω. Energies of other occupied MOs calculated with the Ladder H model also are in a good agreement with HF orbital energies, as are the energies of occupied σ MOs obtained with the Ladder C model. The largest discrepancies, about 0.3 eV, are found for longer chains in loose conformations. Figure 5 shows that the orbital shapes and nodal properties, too, are very similar in the DFT and in the Ladder model calculations, although the size and distribution of the islands observed in the HOMO at small values of ω are not identical (the KS HOMO is of a different symmetry than those in the Ladder models, and this is due to a different MO energy ordering within a tightly packed group of MOs). The general agreement is not surprising, since the parameters in the Ladder models were chosen by fitting HF energies of occupied MOs, albeit over a limited range of conformations[19] (the KS orbital energies are 2.0 to 3.0 eV higher than HF energies and have been shifted up by 2.3 eV in Figure 6). The results shown in Figures 5 and 6 justify the use of the simple Ladder models in our effort to find an intuitive explanation of the origin of the strong conformational effects on σ delocalization in oligosilanes.

The partition ratio values $p_{\mathrm{HOMO}}$ obtained from Ladder C calculations (Figure 7) provide a quantitative measure of σ delocalization and confirm the qualitative conclusions reached so far. Its high value in the $\omega = 180^\circ$ limit marks a high degree of σ delocalization, and it remains high down to about ~90°. At smaller dihedral angles, it drops precipitously. It is interesting to note its quasiperiodic dependence on $n$ in the $\omega = 0^\circ$ limit, which reflects the growth in the number of high amplitude islands as the chain grows longer.

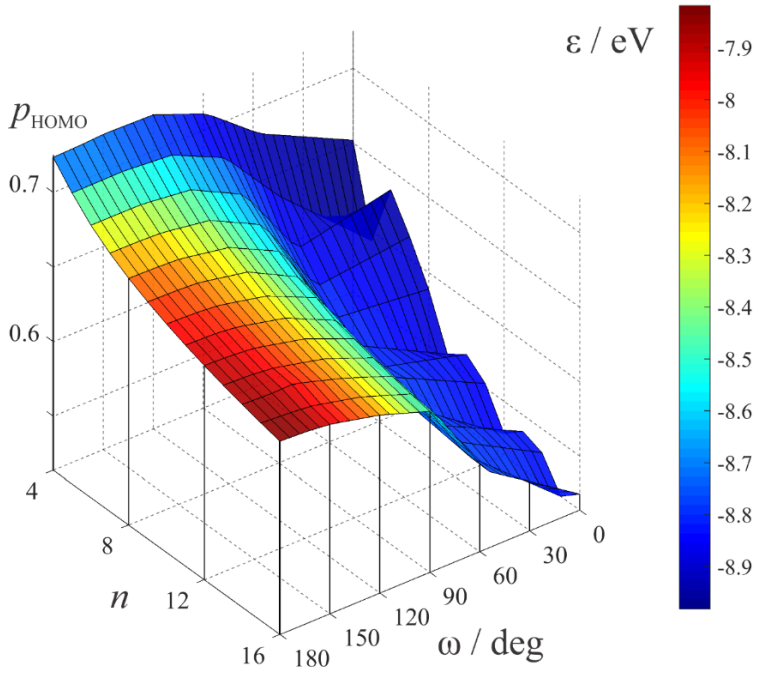


**Figure 7.** The HOMO partition ratio of all-[ω]-**1[*n*]** (*n* = 4 - 16) in Ladder C model (color indicates HOMO energy).

The qualitative similarity of the HF, KS, Ladder H, and Ladder C HOMO orbital energy behavior as a function of *n* and ω is illustrated in more detail in Figure 8. In the loose helix limit, the HOMO energy is sensitive to chain length. In the tight helix limit, all four methods agree that the HOMO energy changes only slightly as the chain length increases. In the region ω = 90 - 120° the two limiting cases meld into each other, with the loose helix characteristics dominant. The tight helix behavior does not dominate fully until ω is reduced to about 60°. Even the largest qualitative difference between the conclusions drawn from the Ladder models and those drawn from the DFT and HF methods is only tiny. In the former, for any *n* the maximum of the HOMO energy is at the all-anti conformation (ω = 180°) whereas in the latter, it is at the all-transoid conformation (ω = 163°).

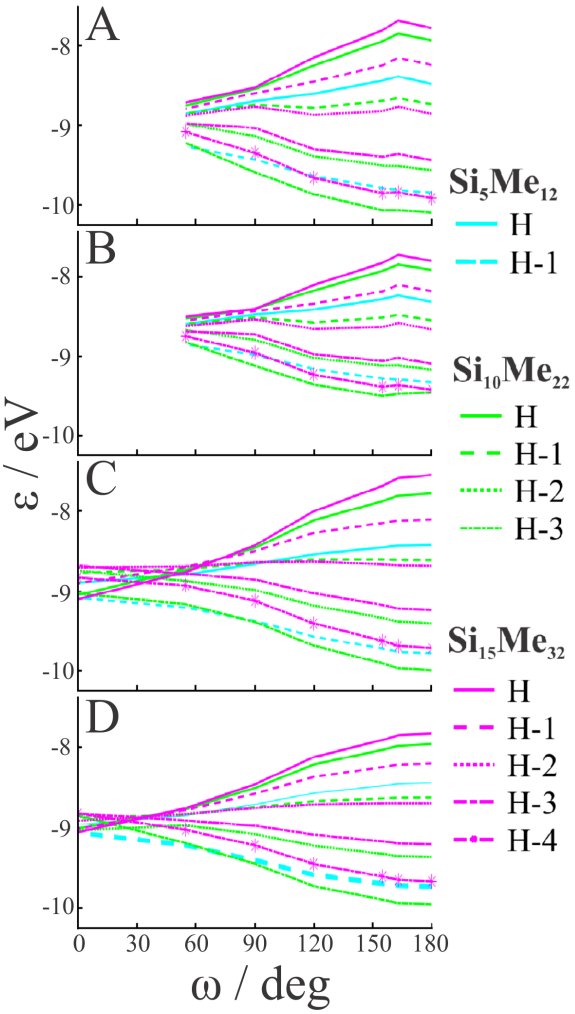


**Figure 8**. Energies of several highest occupied MOs in $Si_5Me_{12}$, $Si_{10}Me_{22}$, and $Si_{15}Me_{32}$ as a function of ω, calculated with HF/TZ (A), DFT/TZ (B), Ladder H (C) , and Ladder C (D) methods. H stands for HOMO. A constant (-2.3 eV) was added to DFT/TZ orbital energies.

Figure 8 also shows that the similarity of the trends displayed by DFT calculations and those obtained with the Ladder methods extends to lower energy orbitals. All four computational methods

show that the width of the band of occupied σ orbitals increases as the chain length grows, hardly a surprise, but they also show that it does so very much more in the loose helix than in the tight helix limit. In the Ladder model calculations, where the limit $\omega = 0^\circ$ can be reached, the orbital energies actually cross at about 30 - 40° and then invert their order. The conclusions reached are entirely compatible with those reached from DFT excitation energies (Figures 2 and 3), HOMO shapes (Figures 4 and 5) and energies (Figure 6), and from the plot of $p_{\mathrm{HOMO}}$ in Figure 7: in loose helices σ delocalization is strong and chain length matters, whereas in tight helices σ delocalization is weak or absent and chain length hardly matters at all.

Although the Ladder models can thus be used to analyze the effects of σ delocalization in terms of HOMO energies, they cannot be used for predictions of energies of virtual orbitals and of excitation energies, since they do not perform well for the relative energies of σ* and π* unoccupied orbitals and the Hückel approximation of equating excitation energies to orbital energy differences alone is inadequate. In the Ladder C model, σπ* transitions are absent altogether. Ladder H attributes much lower energies to σ* than to π* unoccupied orbitals, all predicted low-energy transitions are pure σσ*, and in this important region all σπ* transitions are missing. This may be due to the absence of electron repulsion terms in the expression that relates excitation energies to orbital energy differences, and could perhaps be corrected by an elaboration of the Ladder H model beyond the Hückel level. At this time we prefer to simply acknowledge that the current version of this model is incapable of describing low-lying excited states of linear oligosilanes properly, and we shall confine our discussion to the properties of the HOMO.

**(v) An Intuitive Rationalization of the Contrast between Loose and Tight Helices**

Why is the nature of the HOMO so different in the loose and the tight helices, making the former strongly σ-delocalized and the latter essentially σ-localized? In the following, we provide an intuitive answer at the level of the Ladder C model, and use the similarity of the results of the several approximations used here to claim the answer is valid generally, at least within a certain range of relative strengths of geminal and vicinal interactions (σ conjugation and σ hyperconjugation). Elsewhere, we shall use solid-state band theory for infinite chains to formulate the explanation more rigorously.

We start by recognizing that the description of a long linear $n$-$Si_nMe_{2n+2}$ chain in which the absolute values $|\omega|$ of all backbone dihedral angles are the same requires only three values of resonance (hopping) integrals: $\beta_p$ (primary), $\beta_g$ (geminal), and $\beta_v(\omega)$ (vicinal). Actually, with $\beta_p$ as the energy unit, the model is fully described by the ratios $g = \beta_g/\beta_p$ and $v(\omega) = \beta_v(\omega)/\beta_p$, which describe the relative importance of σ conjugation and σ hyperconjugation, and strongly depend on the choice on the backbone chemical element, the valence angle within the chain, and the length of the backbone bond. Elsewhere, we consider the range of the $[g,v(\omega)]$ space within which the current conclusions hold, but presently we merely accept the values $g = 0.31$ and $v(\omega)$ ranging from -0.23 at $\omega = 180°$ to 0.17 at $\omega = 0°$ that have been determined for permethylated oligosilanes by fitting to HF MO energies.[19] Thus, the results of the present analysis are valid for standard SiSi bond lengths of ~2.36 Å and SiSiSi valence angles of 114°, typical of permethylated oligosilanes.

We first obtain inspiration from a plot of Ladder C $p_i$ values for all σ(SiSi) MOs of $Si_{16}Me_{34}$ as a function of ω (Figure 9B; the explicit form of all these MOs is shown in Figures 9A and 9C). In the first approximation, the plot has the shape of a tilted saddle, with the highest values (the most σ delocalization) for the highest few energy MOs (and especially, the HOMO) in loose helices and

the lowest few energy MOs in tight helices. Low values (the least σ delocalization) are found for the few lowest energy MOs in loose helices and the few highest energy MOs, including the HOMO, in tight helices. This is as expected, since the degree of σ delocalization in the chain is judged by the properties of the HOMO. Figure 9 shows that the internal structure of the least stable MO in loose helices is similar to that of a much more stable one in tight helices and that the most stable MO in tight helices resembles a much less stable one in loose helices. It thus appears that the order of the MOs is approximately inverted upon going from one to the other conformational limit. Such an inversion would be expected if the relative signs of resonance integrals along the chain differed in the two limiting conformations $\omega = 180°$ and $\omega = 0°$. The only ones that change sign are $\beta_v(\omega)$, characterized by the ratio $v(\omega) = \beta_v(\omega)/\beta_p$. This observation suggests a two-step analysis in which $\beta_g$ is ignored at first, as outlined in the following.

In the first step, we construct an MO energy diagram assuming $g = 0$. In that case, the oligosilane chain separates into two mutually non-interacting linear chains of NHOs containing σ bonds indicated in Figure 10 in violet and green solid lines, respectively. The much weaker vicinal interactions within each chain, also colored violet and green, are indicated as dotted lines. When $n$ is odd, the two chains are identical and each contains $(n - 1)/2$ σ(SiSi) bonds. When $n$ is even, one of the chains contains $n/2$ and the other contains $(n/2) - 1$ σ(siSi) bonds.

The chains are assumed to be long enough for end effects on orbital coefficients and node positions to be negligible and for the difference between $n/2$ and $(n/2) - 1$ to be negligible as well. Each of the two subchains is topologically equivalent to a linear polyene with strongly alternating interaction integrals $\beta_p$ and $\beta_v$. The resulting MO energies are all doubly degenerate (exactly when $n$ is odd and approximately when $n$ is even) and for each value of ω they are located within two

identical vertical bands in the energy diagram for the bonding σ MOs. In Figure 11 these bands are shown in violet and green in both limits, ω = 180° and ω = 0°. In each case, only three energy levels in each chain are shown explicitly: the most stable one at the bottom of the band, the least stable one at the top of the band, and one of the intermediate levels. In Figure 12, we show the Ladder C $p_i$ values for all the MOs in a color code.

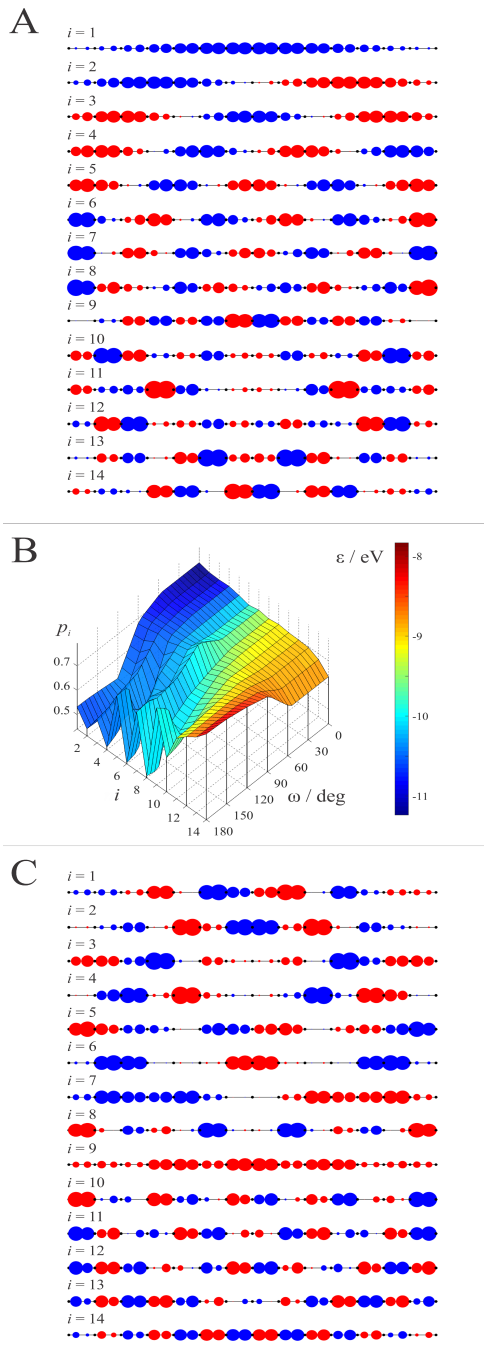


**Figure 9.** All-[ω]-$Si_{15}Me_{32}$ in the Ladder C model: Symbolic representation of the 15 σ(SiSi) MOs at ω = 0° (A) and 180° (C), numbered from the most to the least bonding, and their partition ratio as a function of ω (B, color indicates MO energy).

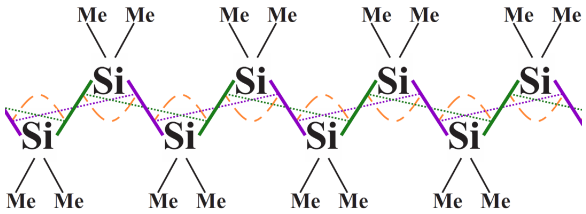


**Figure 10**. Resonance integrals in a permethylated oligosilane chain: primary (full), vicinal (dotted), and geminal (dashed) interactions. The green and violet colors show the division into two equivalent mutually non-interacting linearly conjugated side pieces in the absence of geminal interactions across the ladder rungs (brown).

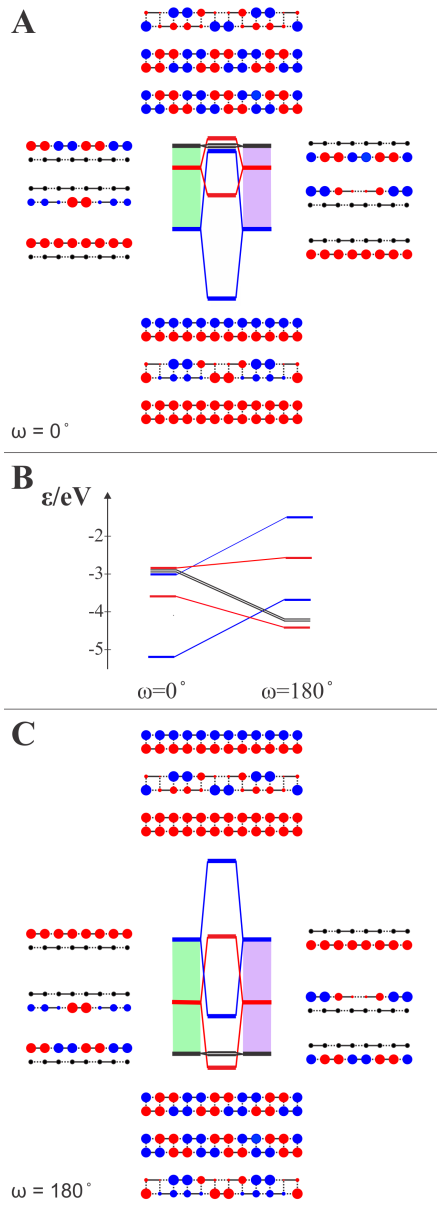


**Figure 11**. Ladder C MO energy diagrams for (A) all-syn (ω = 0°) and (C) all-anti (ω = 180°) conformations of an oligosilane. Orbital energies of two equivalent (odd *n*) or nearly equivalent (even *n*) mutually non-interacting linear chains (green and violet in Figure 8, $v = 0.17$ at all-syn and $v = -0.23$ at all-anti, $g = 0$) on the left (green stack) and right (violet stack). In the middle (white stack), after geminal interactions ($g = 0.31$) are introduced to first order. Schematic orbital structure before interaction is shown on the sides of the diagram, and after interaction, on the top and bottom (the two NHOs on each Si atom are placed above each other, full lines represent primary and dotted lines vicinal interactions). The top to bottom ordering of the orbital sketches after interaction (center) follows the ordering of the orbital energy levels. (B) An all-syn to all-anti correlation diagram showing the energies of selected MOs for oligosilane chain. Dashed lines connect orbitals with identical nodal properties.

The nodal structures of the least stable and the most stable MO within each colored band are shown symbolically, in Figure 11A for the all-syn case $\omega = 0^\circ$ and in Figure 11C for the all-anti case $\omega = 180^\circ$. The MO coefficients are nearly uniform over each non-interacting chain. Their magnitudes and signs at the two NHOs located on each silicon are indicated in color and are shown above each other at the ends of rungs in a long ladder, connected by side pieces in which the primary and the vicinal interactions alternate. The upper side piece contains all the NHOs forming the green set of SiSi bonds in Figure 10 and the lower piece contains all the NHOs that are responsible for the violet set of SiSi bonds. At the moment, there is no interaction across the rungs that connect the two side-pieces. As expected for occupied $\sigma$ bond orbitals, in both the all-anti and the all-syn limit, the signs of the MO coefficients at the two ends of every primary interaction within each oligosilane ladder side piece are equal.

However, because of the difference in the sign of $\beta_v$ at $\omega = 180^\circ$ and $\omega = 0^\circ$, the energy order of the MOs within each colored band is opposite in the two conformations. In the all-anti conformation, $\beta_v > 0$, the least stable MO is the one that has no nodes at all cutting the ladder, and the most stable MO is the one that has a node across each vicinal interaction. In the all-syn conformation, $\beta_v < 0$, and the situation is reversed. Unlike the MOs located at the top or bottom of the colored bands, the MOs whose energy is located inside the colored bands have an intermediate number of nodes and consist of groups of NHOs that carry large amplitudes separated by regions of almost no amplitude, similar to what is seen in Figure 9AC and on the right in Figure 5. One such intermediate energy orbital in each stack is shown explicitly. The $p_i$ values indicated by color in Figure 12 for the same stacks of orbital levels of the subchains make the delocalized nature of the least and the most stable orbitals in each stack and the more localized nature of the orbitals located

at intermediate energies clear.

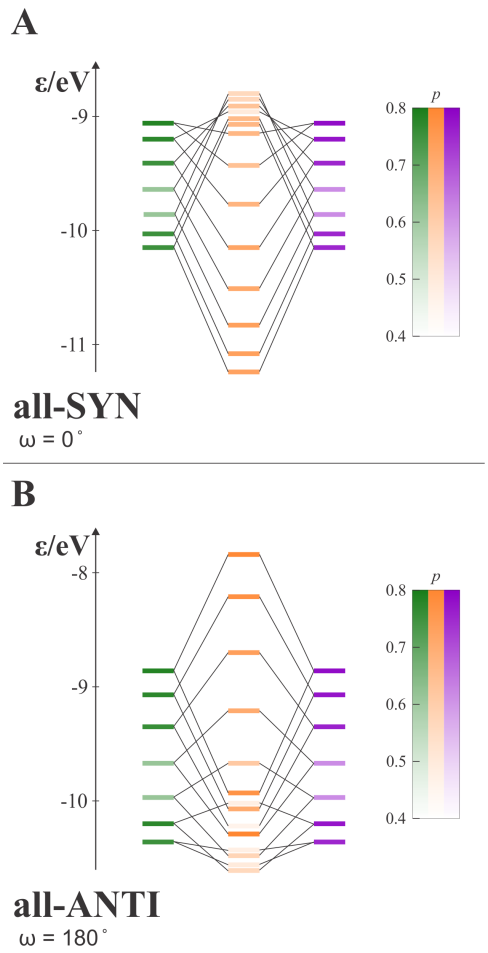


**Figure 12.** Energy diagrams for (A) all-syn and (B) all-anti conformations of $Si_{15}Me_{32}$ in the full Ladder C model: Left and right, MO energies of the green and violet NHO chains (cf. Figure 8) before they are allowed to interact ($g = 0$). Center (orange), MO energies after geminal interactions are introduced ($g \neq 0$). Color shade indicates the partition ratio.

So far, the least bonding (HOMO) and the most bonding among the MOs in the two identical colored stacks of MO levels are both perfectly delocalized and ready to respond to further chain extension, and there is no reason to expect the all-anti conformer to σ delocalize and the all-syn conformer not to do so. This will change in the next step, where we introduce the geminal interactions $\beta_g$ across each of the rungs of the ladder to produce the complete Ladder C Hamiltonian. These cause a formation of in-phase and out-of-phase combinations of degenerate (or nearly degenerate, if *n* is even) levels from the two colored stacks in Figures 11A and 11C, one representing the energies of MOs from the violet side-piece and the other those from the green side-piece. One of these combinations is stabilized and the other is destabilized, and the results are shown in the central column. In the first approximation, the formation of the sums and differences will not affect the relative $p_i$ values over the now doubled number of sites *m*. However, the splitting changes orbital energies from their initial values in each subchain, possibly quite significantly, and introduces the irregularities that appear in the loose helix limit in Figure 9.

In the first approximation, the magnitude of each splitting is dominated by the match of the nodal properties of the MOs in the two colored columns as the summation of interactions over all rungs (Si atoms) in the molecule is performed (Figure 11). The least stable MO in the all-anti case and the most stable MO in the all-syn case, which contain no nodes, are matched perfectly and give the largest splitting. The most stable MO in the all-anti case and the least stable MO in the all-syn case are perfectly mismatched, the contributions from adjacent rungs cancel, and the summation over all rungs yields zero. As a result, for these levels the contributions from the violet and the green side-pieces will still mix even in first order, but their energies will not change at all. For MOs whose energies lie between the two extremes the splitting will be of intermediate size, and one such

example is shown for both the all-anti and the all-syn case. In Figure 12, we show the MO energies that result from the full diagonalization and it is seen that the pattern corresponds to that obtained in the first-order approximation in Figure 11, but there are differences in the level positions because now mixing with antibonding MOs is taken into account.

What, then, will the HOMO look like? In the all-anti case, Figure 11C leaves no doubt: it will be the destabilized combination of the levels from the violet and green columns, just as anticipated from all four types of calculation performed here. This conformer is σ-delocalized and has a high $p_{\mathrm{HOMO}}$ value. Inspection of its uniformly delocalized HOMO makes it clear that further extension of the oligosilane chain will lead to additional destabilization of the HOMO. In the all-syn case, the situation is less clear. The HOMO level could be the doubly degenerate combination of the least stable levels from the violet and green stacks, in which case it would also be fully σ-delocalized, or it could perhaps happen that the interaction of one of the lower-lying degenerate levels, one from the violet and one from the green side piece, will be strong enough to push the resulting destabilized combination even higher and cause it to become the HOMO. This combination will then possess some intermediate number of nodes and will look like the MOs on the right-hand side of Figure 6B, which contain several mutually almost non-communicating regions of large amplitude. Just how many nodes there will be and how large the regions will be is likely to depend strongly on the details of the situation and cannot be stated in general. An extension of the chain will then merely add one or more nearly non-interacting regions and this conformer will be σ-localized.

Which of the situations occurs will depend on the values of $v(\omega)$ and $g$ and we shall address elsewhere in a more quantitative fashion the infinite chain limit and the ranges of values in which

one or the other outcome prevails. The use of standard Ladder C parameters for oligosilanes[19] predicts that the all-syn limit will be σ-localized, as indicated in Figures 9, 11 and 12. The orbital level correlation between the ω = 0° and 180° is shown in Figure 11B and provides a simple explanation of the main features of Figure 8.

The origin of the difference in σ electron delocalization between the all-anti and all-syn limits in permethylated oligosilanes is now clear. In general, the relative importance of geminal and vicinal interactions (σ conjugation and σ hyperconjugation) will be critical in determining the outcome. Note that only the absolute value |ω| enters into the arguments and the sense of the local helicity does not.

**Discussion**

**All-*t* and All-[*ca*] Conformers.** The experimental results for these conformers validate the TD-DFT B3LYP/TZ method of calculation of the dependence of the singlet excitation energies on chain length for two extreme cases: strong dependence on chain length in the all-*t* conformer series (strong σ delocalization), and independence of chain length in the all-[*ca*] conformer series (no σ delocalization). Figure 1 shows that the computations reproduce the behavior of the energy and the intensity of the first observed absorption maximum in samples with random sense of helicity quite well. It is also known that they perform well for the weak transitions in $Si_3Me_8$[22] and a few tetrasilanes[4,22,25] and hexasilanes,[49] and it is reasonable to assume that the TD-DFT B3LYP/TZ level of computation also describes the regular helical conformers correctly.

**Regular Helical Conformers.** With the exception of the all-*t* conformers (ω = 163°), where the agreement with measurements on conformers with a random helical sense (|ω| = 163°) is

excellent (Figure 1), the results shown in Figures 2 and 3 represent predictions. At low energies, they are likely to be quite dependable, but above 50 000 $cm^{-1}$ Rydberg states are likely to intervene and the results cannot be trusted to nearly the same degree. Therefore, we focus our discussion on the 1*B*, 2*A*, 3*A*, and 2*B* excited states. The course of the energies of the 2*B* and 3*A* states as a function of *n* shows irregularities that appear to be due to avoided crossings with higher energy states, but we do not discuss these in detail since as stated we suspect that in this energy range the results are not dependable.

The conformational dependence of the predicted spectra of regular helical conformers thus is vaguely reminiscent of the response of oligosilanes to chain length doubling, discussed earlier[25] in terms of the Ladder C model. A doubling of the number of SiSi bonds causes almost the same red shift of the σσ* transition as long as the two newly created internal dihedral angles remain in the range 180 - 120° (σ-delocalized conformations), and this is followed by an abrupt change to a much smaller or no red shift as the angles become smaller (σ-localized conformations).

**The Difference between the Loose-Helix and Tight-Helix Oligosilane Chromophores**. In common parlance, the loose-helix oligosilanes are σ-delocalized ("σ-conjugated") and the tight-helix oligosilanes are not. This puzzling experimentally observed behavior is faithfully predicted by the present calculations and its origin is now qualitatively clear from a consideration of the all-anti and all-syn limits for a helical chain. The key to the simple understanding is provided by the consideration of an intermediate approximation in which geminal interactions are neglected and the ladder arrangement of approximate $sp^3$ hybrids in the oligosilane chain is split into two non-interacting side pieces that are topologically equivalent to two polyenes with strongly alternating bond lengths (if *n* is odd, each side piece contains half of the Si-Si bonds, and if *n* is even, one side

piece is one bond longer). A change of sign of the vicinal resonance integral $\beta_v$ that is induced by going from loose to tight helices inverts the energy order of the MOs in each side piece. As a result, when the geminal interaction is finally introduced, the MOs that combine to produce the HOMO are very different in the two types of helices. In loose helices ($\beta_v > 0$), there is no doubt that the HOMO will be fully σ delocalized. In tight helices ($\beta_v < 0$), depending on the values of *v* and *g* that characterize the strengths of geminal (σ conjugation) and vicinal (σ hyperconjugation) interactions, the HOMO could have a node at every other Si atom and still be fully delocalized, or it could have an intermediate number of nodes and be fragmented into a series of mutually nearly non-interacting islands, producing a σ-localized system. For oligosilanes, the values of *v* and *g* are such that the latter situation obtains.

In a separate publication, we consider the application of the Ladder C model to an infinite chain in a more quantitative fashion and examine the range of parameters *g* and *v*(ω) within which the distinction between σ-delocalized and σ-localized behavior as a function of conformation applies. This work will build on prior work on helical structures in infinite solids.[50-52]

**Conclusions**

The present work has led to two conclusions: (i) The B3LYP/6-311G**//MP2/6-311G** TD-DFT method reproduces correctly both the strong chain-length dependence of the first singlet excitation energy in peralkylated all-*t* oligosilanes and its near chain-length independence in peralkylated all-[*ca*] oligosilanes (in both types of measured samples, the sense of local helicity is random). This method of calculation should be useful for computing vertical excitation energies of various conformers of peralkylated oligosilanes in general. (ii) The origin of the predicted strong

dependence of the excitation energies and ionization potentials of peralkylated regular helical oligosilanes on the skeletal dihedral angle ω is easy to understand in intuitive terms by consideration of a correlation diagram between two limiting chromophores, the σ-delocalized real all-*a* (ω = 180°) and the σ-localized purely hypothetical all-*c* (ω = 0°). The key to the simple description is the consideration of the interaction of two linearly conjugated structures, each built from half of the σ(SiSi) bonds present, when σ conjugation (geminal interactions) is introduced.

**Acknowledgment**. This work was supported by the US National Science Foundation (CHE 1566435). We are grateful to Prof. Roland Mitric for drawing our attention to the partition ratio index.

**Keywords.** oligosilanes, electronic states, silicon, conjugation, electron delocalization

**References**


1. R. D. Miller, J. Michl *Chem. Rev.* **1989**, *89*, 1359-1410.

2. J. Michl, R. West in *Silicon-Containing Polymers* (Eds.: R. G. Jones, W. Ando, J. Chojnowski), Kluwer Academic Publishers, Dordrecht, The Netherlands, **2000**, p. 499-530.

3. N. Matsumoto, H. Suzuki, H. Miyazaki in *Silicon-Containing Polymers* (Eds.: R. G. Jones, W. Ando, J. Chojnowski), Kluwer Academic Publishers, Dordrecht, The Netherlands, **2000**, pp. 531-552.

4. F. A. Fogarty, D. L. Casher, R. Imhof, T. Schepers, D. W. Rooklin, J. Michl *Pure Appl. Chem.* **2003**, *75*, 999-1020.

5. P. T. Trefonas III, J. R. Damewood, R. West, R. D. Miller *Organometallics* **1985**, *4*, 1318-1319.

6. L. H. Harrah, J. M. Zeigler *J. Polym. Sci., Polym. Lett. Ed.* **1985**, *23*, 209-211.

7. H. Kuzmany, J. F. Rabolt, B. L. Farmer, R. D. Miller *J. Chem. Phys.* **1986**, *85*, 7413-7422.

8. T. Sanji, K. Sakamoto, H. Sakurai, K. Ono *Macromolecules* **1999**, *32*, 3788-3794.

9. S. S. Bukalov, L. A. Leites, R. West *Macromolecules* **2001**, *34*, 6003-6004.

10. F. C. Schilling, F. A. Bovey, D. D. Davis, A. J. Lovinger, R. B. Macgregor, C. A. Walsh, J. M. Zeigler *Macromolecules* **1989**, *22*, 4645-4648.

11. K. Song, R. D. Miller, G. M. Wallraff, J. F. Rabolt *Macromolecules* **1992**, *25*, 3629-3632.

12. M. Fujino, T. Hisaki , N. Matsumoto *Macromolecules* **1995**, *28*, 5017-5021.

13. C.-H. Yuan, R. West *Chem. Commun.* **1997**, 1825-1826.

14. K. Oka, N. Fujiue, S. Nakanishi, T. Takata, T. Dohmaru, C.-H. Yuan, R. West *Chem. Lett.* **1997**, 253-254.

15. K. Oka, N. Fujiue, T. Dohmaru, C.-H. Yuan, R. West *J. Am. Chem. Soc.* **1997**, *119*, 4074-4075.

16. T. A. Su, H. Li, M. L. Steigerwald, L. Venkataraman, C. Nuckolls, *Nat. Chem.* **2015**, *7*, 215-220.

17. K. A. Klingensmith, J. W. Downing, R. D. Miller, J. Michl *J. Am. Chem. Soc.* **1986**, *108*, 7438-7439.

18. H. Teramae, J. Michl *Mol. Cryst. Liq. Cryst.* **1994**, *256*, 149-159.

19. T. Schepers, J. Michl *J. Phys. Org. Chem.* **2002**, *15*, 490-498.

20. M. K. Raymond, J. Michl *Int. J. Quantum Chem.* **1999**, *72*, 361-367.

21. H. Tsuji, M. Terada, A. Toshimitsu, K. Tamao *J. Am. Chem. Soc.* **2003**, *125*, 7486-7487.

22. D. W. Rooklin, T. Schepers, M. K. Raymond-Johansson, J. Michl *Photochem. Photophys. Sci.* **2003**, *2*, 511-517.

23. H. Plitt, J. Michl *Chem. Phys. Lett.* **1992**, *198*, 400-405.

24. M. Kumada, K. Tamao *Adv. Organomet. Chem.* **1968**, *6*, 19-117.

25. A. Bande, J. Michl *Chem. Eur. J.* **2009**, *15*, 8504-8517.

26. B. Albinsson, H. Teramae, H. S. Plitt, L. M. Goss, H. Schmidbaur, J. Michl *J. Phys. Chem*. **1996**, *100*, 8681-8691.

27. A. Reed, L. Curtiss, F. Weinhold *Chem. Rev.* **1988**, *88*, 899-926.

28. W. Kutzelnigg *J. Mol. Struct. (Theochem)* **1988**, *169*, 403-419.

29. F. Wegner *Z. Physik B* **1980**, *36*, 209-214.

30. I. V. Alabugin, K. M. Gilmore, P. W. Peterson *WIRES Comput. Mol. Sci.* **2011**, *1*, 109-141.

31. I. V. Alabugin, *Stereoelectronic Effects: A Bridge Between Structure and Reactivity* 1st ed., John Wiley & Sons, Ltd., Oxford, UK, **2016**.

32. C. Sandorfy *Can. J. Chem.* **1955**, *33*, 1337-1351.

33. A. Herman *Chem. Phys.* **1988**, *122*, 53-61.

34. R. Ahlrichs, M. Bär, H. P. Baron, R. Bauernschmitt, S. Böcker, M. Ehrig, K. Eikorn, S. Elliot, F. Furche, F. Haase, M. Häser, H. Horn, C. Huber, U. Huniar, M. Kattaneck, C. Kömel, M. Kollwitz, K. Kay, C. Ochsenfeld, H. Ohm, A. Schäfer, U. Schneider, O. Treutler, M. von Arnim, F. Weigend, P. Weis, H. Weiss *Turbomole*, **1988**.

35. J. Michl, R. West *Acc. Chem. Res.* **2000**, *33*, 821-823.

36. M. J. Frisch, et al. *Gaussian 03, Revision C.02*, Gaussian, Inc., Wallingford CT, **2004**.

37. R. E. Stratmann, G. E. Scuseria, M. Frisch *J. Chem. Phys.* **1998**, *109*, 8218-8224.

38. M. J. Frisch, et al. Gaussian, Inc., Wallingford CT, **2009**.

39. E. D. Glendening, J. K. Badenhoop, A. E. Reed, J. E. Carpenter, F. Weinhold *NBO 3.1.*; Theoretical Chemistry Institute, University of Wisconsin, Madison, **1996**.

40. E. D. Glendening, J. K. Badenhoop, A. E. Reed, J. E. Carpenter, J. A. Bohmann, C. M. Morales, F. Weinhold *NBO 5.0.*; Theoretical Chemistry Institute, University of Wisconsin, Madison, **2001**.

41. *MATLAB*, Version 7.9 (R2011b), The Math Works, Inc., **2011**.

42. H. Gilman, W. H. Atwell, G. L. Schwebke *Chem. Ind. (London)* **1964**, 1063.

43. H. Gilman, W. H. Atwell, G. L. Schwebke *J. Organomet. Chem.* **1964**, *2*, 369-371.

44. H. Sakurai, R. Koh, A. Hosomi, M. Kumada *Bull. Soc. Chem. Jpn.* **1964**, *39*, 2050-2051.

45. H. S. Plitt, J. W. Downing, M. K. Raymond, V. Balaji, J. Michl *J. Chem. Soc., Faraday Trans.* **1994**, *90*, 1653-1662.

46. K. Obata, M. Kira *Organometallics* **1999**, *18*, 2216-2222.

47. S. Mazières, M. K. Raymond, G. Raabe, A. Prodi, J. Michl *J. Am. Chem. Soc.* **1997**, *119*, 6682-6683.

48. M. K. Raymond Ph. D. Dissertation, University of Colorado, **1997**.

49. Y. Kanazawa, H. Tsuji, M. Ehara, R. Fukuda, D. L. Casher, K. Tamao, H. Nakatsuji, J. Michl *ChemPhysChem* **2016**, *17*, 3010-3022.

50. I. Bozovic *Phys. Rev. B* **1984**, *29*, 6586.

51. W. H. Glassey, R. Hoffmann *Theor. Chem. Acc.*, **2002**, *107*, 272-281.

52. M. Rahm, J. I. Lunine, D. A. Usher, D. Shalloway Proc. *Natl. Acad. Sci. U.S.A*. **2016**, *113*, 8121-8126.

TOC Graphic:

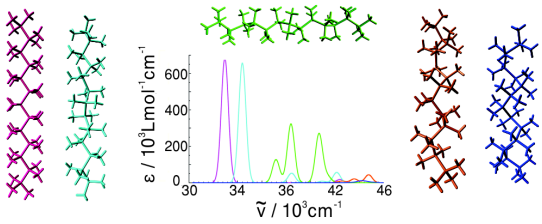


**Why Stretch the Coil?**

The HOMO energy and UV absorption spectrum of a uniformly helically coiled oligosilane respond to chain elongation by a strong shift when the coil is extended and do not respond at all when the coil is compressed. Why are σ(SiSi) electrons in the HOMO delocalized in a loose helix and localized in a tight helix? We provide an intuitive explanation at the Hückel level.